Cellular/Molecular

PMCA2 via PSD-95 Controls Calcium Signaling by α7-Containing Nicotinic Acetylcholine Receptors on Aspiny Interneurons

David Gómez-Varela,[1] **Manuela Schmidt,**[2] **Jeff Schoellerman,**[1] **Eric C. Peters,**[3] **and Darwin K. Berg**[1]

[1]Division of Biological Sciences, University of California, San Diego, La Jolla, California 92093-0357, [2]The Scripps Research Institute, La Jolla, California 92037, and [3]Genomics Institute of the Novartis Research Foundation, San Diego, California 92121

Local control of calcium concentration within neurons is critical for signaling and regulation of synaptic communication in neural circuits. How local control can be achieved in the absence of physical compartmentalization is poorly understood. Challenging examples are provided by nicotinic acetylcholine receptors that contain α7 nicotinic receptor subunits (α7-nAChRs). These receptors are highly permeable to calcium and are concentrated on aspiny dendrites of interneurons, which lack obvious physical compartments for constraining calcium diffusion. Using functional proteomics on rat brain, we show that α7-nAChRs are associated with plasma membrane calcium-ATPase pump isoform 2 (PMCA2). Analysis of α7-nAChR function in hippocampal interneurons in culture shows that PMCA2 activity limits the duration of calcium elevations produced by the receptors. Unexpectedly, PMCA2 inhibition triggers rapid calcium-dependent loss of α7-nAChR clusters. This extreme regulatory response is mediated by CaMKII, involves proteasome activity, depends on the second intracellular loop of α7-nAChR subunits, and is specific in that it does not alter two other classes of calcium-permeable ionotropic receptors on the same neurons. A critical link is provided by the scaffold protein PSD-95 (postsynaptic density-95), which is associated with α7-nAChRs and constrains their mobility as revealed by single-particle tracking on neurons. The PSD-95 link is required for PMCA2-mediated removal of α7-nAChR clusters. This three-component combination of PMCA2, PSD-95, and α7-nAChR offers a novel mechanism for tight control of calcium dynamics in neurons.

Introduction

Calcium is a key regulator of numerous biological processes in neurons. To achieve specificity, cells must tightly control the amount, time course, and spatial distribution of calcium elevations. A common strategy is to confine calcium influx to critical sites by means of protein–protein interactions that severely restrict the location of channels mediating the flux, as in the case of voltage-gated calcium channels at presynaptic terminals (Kaeser et al., 2011). Physical compartmentalization of the incoming calcium offers another mechanism, as seen for dendritic spines where intracellular diffusion is limited by the narrow spine neck

(Yuste, 2011). A third strategy is to impose multiple channel-opening conditions that limit activation to special physiological circumstances. This is the case for calcium-permeable NMDA receptors, which, for activation, require membrane depolarization, the agonist glutamate, and a coagonist (Dingledine et al., 1999). These strategies can be combined, as exemplified by NMDA receptors constrained at postsynaptic sites on spines (Schiller et al., 1998; Yuste et al., 1999).

Apparently unconstrained by such strategies are homopentameric α7-containing nicotinic acetylcholine receptors (α7-nAChRs). These are widely expressed but are not confined to compartments, such as spines, though the receptors have a high relative calcium permeability (Bertrand et al., 1993; Séguéla et al., 1993) and regulate calcium-dependent events (Jones et al., 1999; Dajas-Bailador and Wonnacott, 2004; Dickinson et al., 2007; Albuquerque et al., 2009; Miwa et al., 2011). Further, they require only the agonist acetylcholine for activation and may even participate in "volume transmission," responding to transmitter diffusely distributed (Descarries et al., 1997). Most challenging are the relatively high numbers of α7-nAChRs found on dendritic shafts of hippocampal aspiny interneurons (Khiroug et al., 2003; Fayuk and Yakel, 2007), where the receptors have been reported to participate in synaptic plasticity (Rózsa et al., 2008). Because interneurons display several forms of pathway-specific synaptic plasticity (Kullmann and Lamsa, 2007), they must carefully regulate local calcium dynamics. How can substantial calcium influx, as mediated by α7-nAChRs, be permitted and yet controlled in such cases?

Performing functional proteomics, we show here that α7-nAChRs are functionally linked to the plasma membrane calcium-ATPase pump isoform 2 (PMCA2) on interneurons via the scaffold protein PSD-95 (postsynaptic density-95). PMCA2 controls the extrusion of calcium upon α7-nAChR activation. Remarkably, blockade of PMCA2s, by rapidly decreasing the number of α7-nAChR clusters on the cell surface, causes a substantial decrease in the magnitude of α7-nAChR-dependent calcium transients. This decrease does not occur if PSD-95 levels are reduced by RNA interference (RNAi). Single-particle tracking (SPT) studies using quantum dots (QDs) indicate that PSD-95 constrains α7-nAChR movements on the cell surface, placing the receptors under PMCA2 control. If pump activity is compromised, the PSD-95 link enables the cell to reduce the number of α7-nAChR clusters.

Materials and Methods

Isolation of α7-nAChR complexes from rat brain. Ten postnatal day 9 (P9) rat brains of either sex were homogenized (10 s driller pulse on ice) with ice-cold solubilization buffer (SB; 4 ml/g brain tissue; 5 g total) containing (in mM): 150 Tris-HCl, pH 8; 100 NaCl; 0.5 EDTA; and glycerol 10%. After centrifuging at 3800 rpm for 8 min at 4°C, the supernatant fraction was collected and saved on ice; the pellet was suspended in ice-cold SB (1.3 ml/g brain tissue) and centrifuged again at 3800 rpm for 8 min at 4°C. The two supernatant fractions were pooled and centrifuged at 45,000 rpm for 40 min at 4°C. The resulting pellet fraction was resuspended in ice-cold SB containing 0.5% sodium-deoxycholate and 0.5% Nonidet P-40 (NP-40; 500 μl/g brain tissue) and homogenized by 20 strokes with a P1000 micropipette, followed by 20 strokes with a P200 micropipette. The resulting suspension was incubated 2 h at 4°C on a horizontal shaker at 210 rpm and then centrifuged at 45,000 rpm for 40 min at 4°C. The resulting supernatant fraction (500 μl) was incubated with 40 μl of α-bungarotoxin (Bgtx) beads overnight at 4°C with gentle rotation. Bgtx beads were prepared by coupling α-bungarotoxin (Invitrogen) to Actigel ALD (Sterogene Bioseparation) using the manufacturer's protocol. Negative controls included either substitution of unconjugated beads for the Bgtx beads or addition of 1 mM nicotine to the solution before applying to the Bgtx beads. The beads were then collected by centrifugation at 5000 rpm for 1 min and washed six times by gentle rotation for 10 min at 4°C with 1 ml aliquots of ice-cold SB containing 150 mM NaCl plus 0.5% sodium deoxycholate and 0.5% NP-40 before recentrifugation. Absorbed proteins were then eluted by incubating 10 min at 75°C in 40 μl of elution buffer containing: 1× lithium dodecyl sulfate sample buffer (Thermo Scientific) and 1× NuPAGE sample reducing agent (Invitrogen). The resulting mixtures were resolved by one-dimensional SDS-PAGE, and each resolved lane was cut into 16 equal gel slices, which were analyzed separately by mass spectrometry.

Mass spectrometry. Excised gel bands were subjected to in-gel digestion using a Micromass MassPREP Station in conjunction with the manufacturer-specified protocols. Briefly, gel pieces were rinsed (2× with 50% acetonitrile/50 mM ammonium bicarbonate), dehydrated (acetonitrile), reduced (dichloro-diphenyl-trichloroethane), alkylated (iodoacetamide), and digested with sequencing grade trypsin overnight. The resulting peptides were extracted with 30 μl of 1% formic acid. Automated nanoscale liquid chromatography–tandem mass spectrometry was performed using a ThermoFinnigan Surveyor HPLC and LTQ Orbitrap ion trap mass spectrometer along with a variation of the "vented column" approach. Ten microliters of a tryptic digest extract was loaded onto a 5 cm long × 75 μm inner diameter precolumn packed with 5 μm C-18 silica (Monitor 100Å) retained by a Kaisel frit. After thorough washing, the vent was closed and, by starting the reversed-phase run, the sample was transferred to a 12 cm long × 75 μm inner diameter column with a pulled 5 μm tip packed with the same material. The chromatographic profile was from 100% solvent A (0.1% acetic acid) to 50% solvent B (0.1% acetic acid in acetonitrile) in 30 min at ~200 nl/min (manual split from 300 μl/min), and also allowed for appropriate times for column washing and reequilibration. An angiotensin 1 standard (1.25

pmol) was run between each sample to eliminate carryover as well as monitor overall system performance. The LTQ Orbitrap acquisition method involved one mass spectrometry (MS) precursor ion scan followed by five data-dependent tandem MS scans. Dynamic exclusion was enabled for a repeat count of 1 s, repeat duration of 15 s, and exclusion duration of 30 s.

Database search. Tandem MS data were used to search a rat-specific database with an appended reverse sequence copy (EBI-IPI_rat_3.36 database, 82,502 entries) using Sequest (version 3.0; ThermoFinnigan). Searches were performed allowing for the fixed modification of cysteine (carbaminomethyl), the variable modifications of Met (oxidation), and no enzyme specificity. Scaffold (version Scaffold_3_00_02; Proteome Software) was used to validate tandem MS-based peptide and protein identifications. Peptide identifications were accepted if they could be established at >95.0% probability as specified by the Peptide Prophet algorithm (Keller et al., 2002). Protein identifications were accepted if they could be established at >99.9% probability and contained at least two identified peptides. Protein probabilities were assigned by the Protein Prophet algorithm (Nesvizhskii et al., 2003).

DNA constructs. Mouse PMCA2 (clone 30621322, Openbiosystems) was extracted from the pYX-Asc vector using appropriate oligonucleotides to ligate the PMCA2 cDNA between the EcoR1/XhoI sites of the multiple cloning site of pcDNA 3.1/Myc-His vector (Invitrogen). The point mutations in the PDZ (PSD-95/Discs large/zona occludens-1) domains of the CD4-α7 loop were made using the QuikChange Lightning Site-Directed Mutagenesis kit (Agilent Technologies). The primer pairs to change both PDZ domains were the same as described previously (Baer et al., 2007). All constructs were verified by sequencing. Silencing of rat PMCA2 was done by using a SureSilencing short hairpin RNA (shRNA) plasmid (catalog number KR52851G). SAP-102-XFP (synapse associated protein-102-XFP), sh95-XFP, and shScr95-XFP were generated as previously described (Conroy et al., 2003; Neff et al., 2009).

HEK293 transfections. HEK293 (human embryonic kidney 293) cells were transferred from a 75 cm² bottle at confluency to 10 cm plates (Corning) at a 1:9 dilution. Cells were transfected by adding 1 ml/plate of HEK293 medium (Opti-MEM, Invitrogen) with 20 μl of Fugene/plate (Promega) with either 4 μg of PMCA2-Myc and 8 μg of α7-GFP or 8 μg of CD4 construct. After 3 d, cells were detached from the plates by pipetting PBS buffer and collected by centrifuging at 10,000 rpm for 5 min at room temperature. The cells were lysed by adding lysis buffer (in mM): 0.5 EDTA, 100 NaCl, 10% glycerol, 1% dodecyl-D-maltoside, 50 Tris-Hcl, and 1 protease inhibitors, pH 7.5, and passing through 20 and 25 gauge syringes. After 30–60 min incubation on ice, the lysate was centrifuged 10 min at 10,000 rpm at 4°C to remove insoluble material. Antibodies (Abs) conjugated to beads and recognizing Myc (clone 9E11, Santa Cruz Biotechnology), GFP (A11122, Invitrogen), or CD4 (MEM-241, Santa Cruz Biotechnology) were incubated with the supernatant fraction overnight at 4°C with gentle rotation to bind the corresponding antigen. After three washes with diluted lysis buffer (1:1 dilution), bound proteins were eluted with elution buffer (see above), separated by SDS-PAGE, and transferred to nitrocellulose membranes.

Western blots. For material from transfected HEK293 cells, Western blots were probed with anti-Myc Ab (1:500; clone 9E11, Santa Cruz Biotechnology) or anti-α7-nAChR Ab (1:500; C-20, Santa Cruz Biotechnology), followed by HRP-conjugated secondary Ab (1:2000; Jackson Laboratories). For material from rat brain extracts, the blots were probed with anti-PSD-95 Ab (1:1000; Cell Signaling Technology) or anti-α7-nAChR Ab (1:1000; 1:500; C-20, Santa Cruz Biotechnology) followed by HRP-conjugated secondaries. Antibody binding was detected with ECL reagents (Pierce) and developed with Kodak X-OMAT Blue XB Film.

Hippocampal cultures. Hippocampal cultures were prepared from 18-d-old to 19-d-old Sprague Dawley rat embryos as previously described (Kawai et al., 2002). Briefly, hippocampi were removed rapidly under stereomicroscopic observation, cut into small pieces, and digested with 20 U/ml of trypsin (Invitrogen;) in HBSS Invitrogen at 37°C for 12 min. The tissue segments were then transferred to Neurobasal medium (Invitrogen) with 10% heat-inactivated horse serum (Invitrogen), triturated with a fire-polished Pasteur pipette, and plated at 1×10^5 cells per 12 mm glass coverslip previously coated with poly-D-lysine (>300 kDa; Sigma).
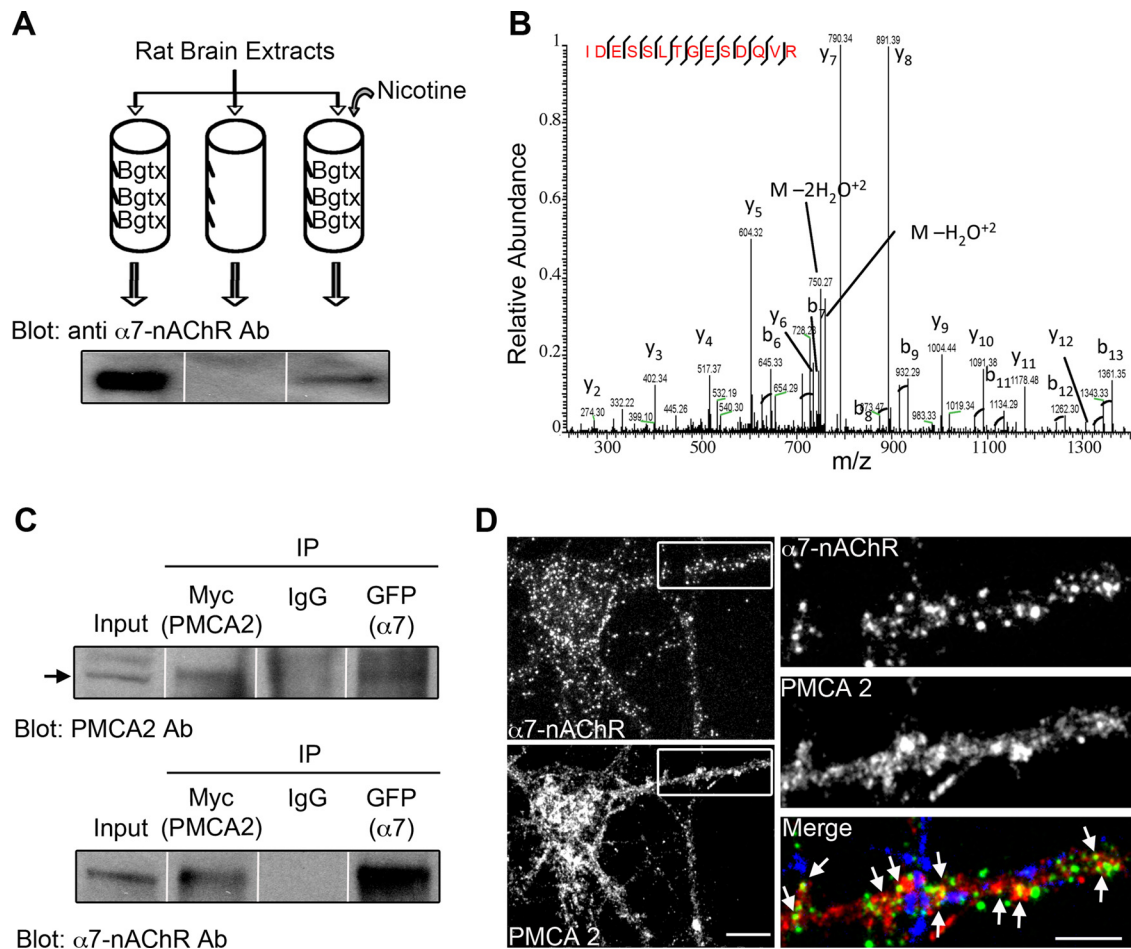
Figure 1. Proteomic analysis reveals PMCA2 associated with α7-nAChRs. **A**, Rat brain extracts were passed through affinity columns containing Bgtx coupled to actigel beads (left), beads alone (middle), or Bgtx beads incubated with nicotine to block specific α7-nAChR binding (right). The specificity of the procedure was confirmed by eluting bound material followed by Western blot probed with anti-α7-nAChR Ab, which identified receptor prominently in the Bgtx bead lane. **B**, Tandem MS spectra of a peptide unique for PMCA2. The fragment y^+-ion and b^+-ion series are indicated together with the amino acid sequence derived from the mass differences (red). **C**, Coimmunoprecipitation of PMCA2 and α7-nAChRs transiently transfected into HEK293 cells. Proteins were immunopurified (IP) with Abs against PMCA2-Myc (Myc), nonspecific Abs (IgG), or against α7-nAChR-GFP (GFP). Arrow indicates the PMCA-Myc band. Similar results were obtained from three independent experiments. **D**, Hippocampal interneurons identified by GAD65 staining (Merge, blue; 15–17 d *in vitro*) were stained for surface α7-nAChRs (green) and PMCA2 (red). Magnified images show colocalization of α7-nAChRs and PMCA2 (Merge, arrows indicate examples). Scale bars: (in PMCA2) left columns, 10 μm; (in Merge) right columns, 5 μm.

Subsequent feeding occurred twice weekly, each time replacing half the volume with fresh Neurobasal media with 2% B-27 (Invitrogen). The cultures were maintained in a humidified tissue culture incubator with 5% CO_2 and taken for use after 15–17 d. Cultures were transfected using the calcium-phosphate method (Clontech; Goetze et al., 2004) on days 7–8.

Immunocytochemistry. For immunostaining, hippocampal neurons in culture were incubated with the indicated compounds (e.g., CX3A, 250 μM, for 1 h at 37°C in hippocampal culture medium) (see above). After three washes with warm culture medium, surface α7-nAChRs were labeled by incubating with Bgtx-Alexa488 (100 nM; Invitrogen) for 30 min at 37°C. After two washes with HEPES buffer, cells were fixed with 2% PFA in PBS for 10 min at room temperature, and then permeabilized by incubating 10 min with 0.1% Triton X-100 in PBS. To label PMCA2, cells were incubated with an anti-PMCA2 Ab (PA1–915, Pierce) for 1 h at room temperature in PBS containing 5% normal donkey serum. PSD-95 and GAD-65 labeling were obtained with anti-PSD-95 Ab (MA1–046, Pierce) and anti-GAD-65 Ab (either GAD-6 antibody from the Hybridoma Bank or AB1511 from Millipore. The GAD-6 antibody developed by Gottlieb was obtained from the Developmental Studies Hybridoma Bank, which was established under the auspices of the National Institute of Child Health and Human Development and is maintained by the University of Iowa, Department of Biology, Iowa City, Iowa), respectively. After washing three times in PBS, cells were incubated with appropriate donkey FITC, Cy3-conjugated secondary Ab, or

Cy5-conjugated secondary Ab 2 h at room temperature (1:250; Jackson ImmunoResearch Laboratories), washed three times with PBS, and mounted on slides for imaging.

Confocal images were acquired in sequential mode using a Leica SP5 confocal microscope with settings that did not saturate the fluorescence signals and that fulfilled Nyquist sampling criteria. ImageJ software was used for quantifying the number of specific protein clusters. Four regions of interest (ROIs) of 20 μm in length were randomly selected per field of view along the dendrites of interneurons, identified by GAD-65 staining. ROIs were binarized automatically using the mean of the background value inside the dendrite plus 3× the SD as an intensity threshold value for defining a cluster or puncta in each image. Clusters (puncta) within an ROI were counted if they had at least 3 × 3 pixels above threshold (pixel diameter, 80 nm). Data are expressed as the mean plus SEM per dendritic length of 20 μm and represent at least six images from each of three or more cultures.

Calcium imaging. Hippocampal neurons in culture were incubated with 5 μM of Fluo-4 (Invitrogen) for 30 min at room temperature in recording medium containing (in mM): 160 NaCl, 10 HEPES, 10 glucose, 4.5 KCl, 2 $CaCl_2$, 1 $MgCl_2$, pH 7.4. Residual dye was removed with three washes using recording medium, and the neurons were incubated an additional 30 min at 37°C to allow equilibration. The neurons were then placed in a recording chamber on the SP5 Leica confocal stage and calcium fluorescence images were obtained at a frequency of 9 Hz using a
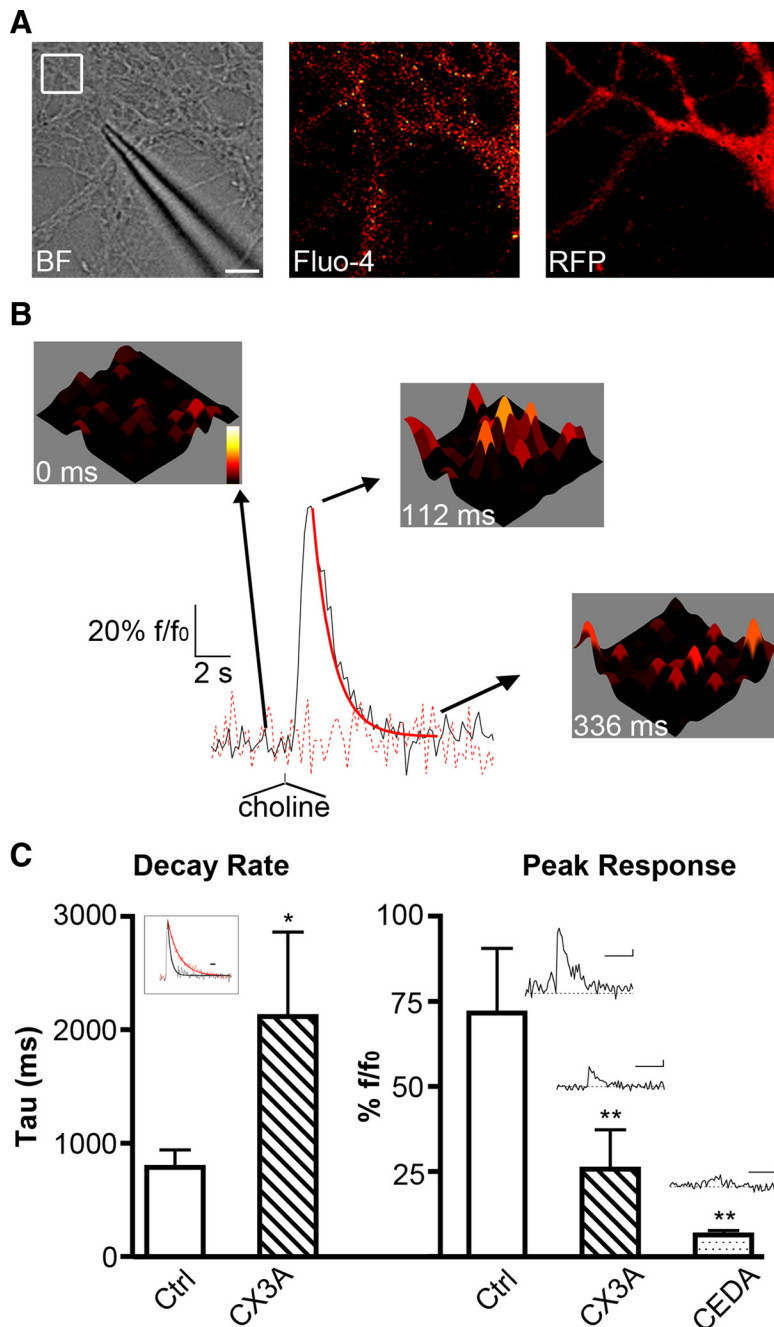
Figure 2. PMCA2 is functionally linked to α7-nAChRs. **A**, Position of the pipette (bright field, BF, left) and basal Fluo-4 fluorescence levels (Fluo-4, middle) on an aspiny neuron transfected with RFP (right) to control for cell volume change artifacts. BF, Inset, Area receiving focal application of choline. Scale bar: 5 μm. **B**, Choline application activates α7-nAChRs, producing a transient calcium elevation. Images show 3D representation of relative calcium levels in a microdomain before (0 ms) and after (112 and 336 ms) choline application. The decay phase of the response was fit with a single exponential (red). **C**, Left, PMCA2 blockade by CX3A slows the decay phase of calcium elevation induced by α7-nAChR activation. Insert shows the comparison of decay kinetics for α7-nAChR-dependent calcium transients in control (black) and CX3A (red), normalized for peak amplitude (790 ± 152 and 2130 ± 754 ms, respectively; *p = 0.033 by two-tailed t test; n = 10–12 interneurons). Scale bar: 2 s. Right, Peak calcium responses induced by α7-nAChR activation in vehicle (Ctrl) versus the PMCA2 inhibitors CX3A and carboxyeosin (CEDA). Inserts show representative traces for the responses (71.5 ± 19, 21.7 ± 11.5, and 6.3 ± 1.3%, respectively; **p = 0.002 by one-way ANOVA with *post hoc* Bonferroni test; n = 10–12 interneurons). Scale bars: vertical, 20%; horizontal, 2 s.

from at least three cultures and at least four neurons per culture. Data are expressed as the mean ± SEM unless otherwise indicated.

Single-particle tracking. QDs (Invitrogen) tethered to individual α7-nAChRs via specific biotinylated ligands were used as fluorescent probes to follow the mobility of nAChRs. Synapses were labeled using MitoTracker 580 staining (100 nM, Invitrogen). MitoTracker Red 580 staining was performed by adding the reagent to the culture medium for 2 min at 37°C and washing two times with culture media. After rinsing three times with PBS containing 0.1% BSA, neurons were incubated with biotinylated Bgtx (Biot-Bgts, 10 nM, Invitrogen) for 10 min on ice, washed three times with PBS plus 0.1% BSA, and then incubated for 5 min with 0.5 nM streptavidin-coated QDs (605 nm) on ice. Cultures were washed three times with recording medium containing (in mM): 160 NaCl, 10 HEPES, 10 glucose, 4.5 KCl, 2 CaCl$_2$, 1 MgCl$_2$, pH 7.4. Negative controls used streptavidin-QDs alone or used 100 μM nicotine to compete with the Biot-Bgtx. To minimize tracking of internalized QD-nAChRs, all movies were confined to a 20 min period immediately after labeling (Charrier et al., 2006). Treating cells with an acid wash (30 s, pH 5.5, at room temperature; Ehlers et al., 2007) removed the vast majority of QDs, confirming that little, if any, internalization had occurred.

Neurons were imaged with an inverted microscope (Zeiss Axiovert 200M) equipped with a 63× oil immersion objective (numerical aperture, 1.40). Samples were illuminated with a mercury lamp and imaged with appropriate excitation filters, dichroic mirrors, and emission filters. Settings were HQ545/30, Q565LP, and HQ610/75M, respectively for Mito-Tracker; D420/40X, 470DCXR, and D605/40, respectively, for QD 605; and HQ487/25, Q505LP, and HQ535/40M, respectively, for GFP. Fluorescence images were acquired with 95 ms exposure times at 10 Hz using a CCD camera (AxioCam MRm, Zeiss) and AxioVision 4.6 software (Zeiss).

Single QDs were identified by their characteristic blinking and were tracked with ImageJ (National Institutes of Health) plug-in Spot-Tracker, after processing image sequences with the SpotEnhancing Filter plug-in (Sage et al., 2005). QD trajectories were sorted into synaptic and extrasynaptic bins. Synapses were identified as boutons staining positive with the mitochondria marker MitoTracker; a punctate region of three pixels in diameter (0.2 μm/pixel) within the labeled space was used to assess QD movement at that synaptic site (Aravanis et al., 2003). QD trajectories were retained only if they contained at least 10 consecutive frames with the center of the QD remaining within the space (synaptic or extrasynaptic) throughout. Frames in which the fluorescence signal disappeared due to blinking of the QD were omitted from the analysis. In such cases, the trajectory was reconstructed by joining trajectory fragments immediately before and after the blink. Instantaneous diffusion coefficients (D_i) were determined for each trajectory as described previously (Gómez-Varela et al., 2010), fitting the first five points of the mean squared displacement

63× (numerical aperture, 0.9) water immersion objective. A brief (50 ms) puff of 1 M choline was delivered locally at 2 psi using a micropipette with 1 μm tip diameter placed 5 μm from the dendritic surface (Fayuk and Yakel, 2007). Increments in fluorescence (*f*) were normalized to the average baseline fluorescence (*f$_0$*) measured during a 1 min period immediately before the application of choline. Recordings were obtained

(MSD) curve versus the lag time. The global localization accuracy was determined by testing the vibrational stability of the setup and calculating MSD for immobile spots. Immobile QDs were defined as streptavidin-QDs stationary on the surface of glass-bottom dishes in the absence of neurons. The localization accuracy was 50 nm, and the resolution limit in terms of diffusion coefficients was 0.008 $\mu m^2/s$.

Feret's diameter was measured as the distance between the two most distal points of a trajectory.

Results

Association of PMCA2 with α7-nAChRs
To identify proteins associated with α7-nAChRs, we affinity-purified protein complexes from rat brain extracts using Bgtx beads. Negative controls included unlinked beads or inclusion of the competitor nicotine along with the Bgtx beads (Fig. 1*A*). Differentially bound proteins were identified by comparative liquid chromatography–tandem mass spectrometry analysis of the retained fractions. Importantly, one protein found only in the Bgtx bead eluate was PMCA2 (Fig. 1*B*). PMCA isoforms are members of a multigene family of high-affinity calcium pumps that are expressed in the brain and extrude calcium from the cytosol (Kozel et al., 1998; Strehler and Zacharias, 2001; Jensen et al., 2007; Strehler et al., 2007). The bait protein α7-nAChR was also found only in the Bgtx bead eluate (data not shown), validating the approach. We verified association of α7-nAChRs with PMCA2 by performing reciprocal coimmunoprecipitation of the two from HEK293 cells transiently transfected with Myc-tagged PMCA2 and GFP-tagged α7-nAChR (Fig. 1*C*). Further, immunostaining of hippocampal interneurons in cell culture revealed a considerable degree of colocalization of the two endogenous proteins (Fig. 1*D*). Together, the results strongly support a previously unrecognized association between α7-nAChRs and PMCA2.
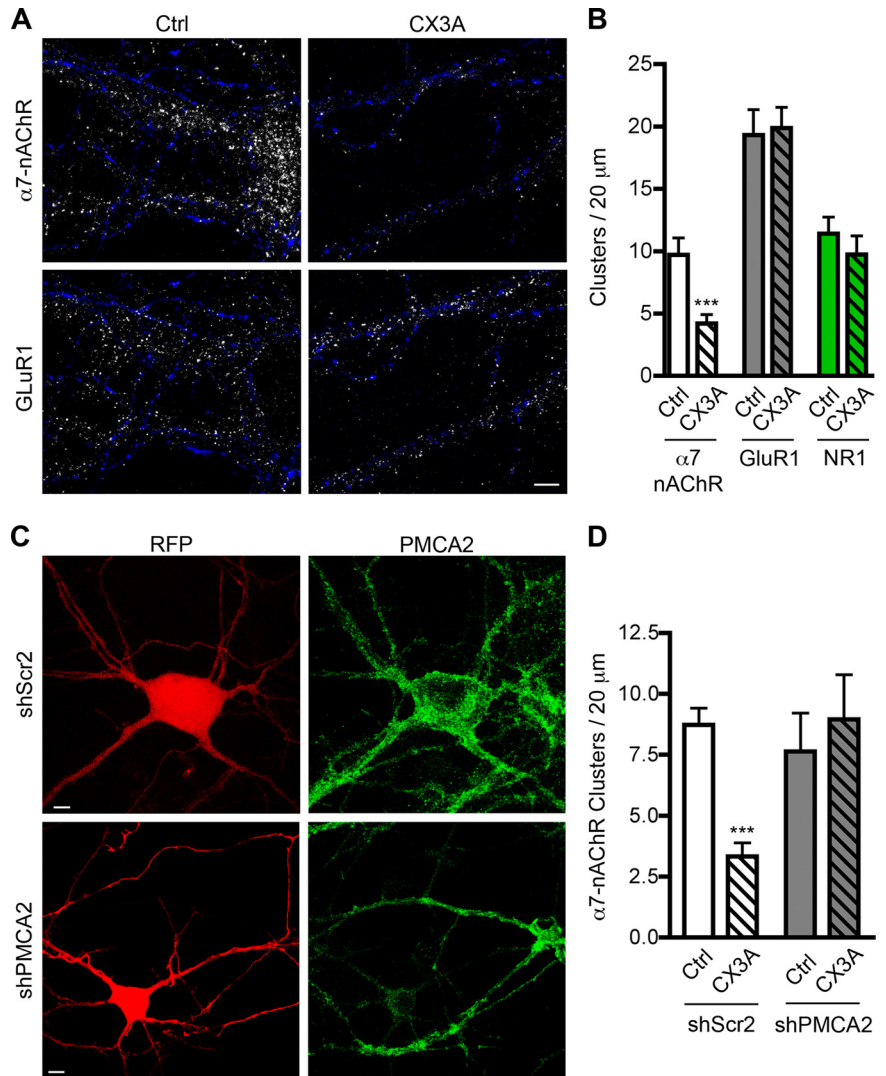
Figure 3. PMCA blockade decreases the number of α7-nAChR clusters on hippocampal interneurons. *A*, Images of α7-nAChR and GluR1 receptor clusters on the surface of the same interneurons (GAD65, blue) in either control (Ctrl) or CX3A. Scale bar: 10 μm. *B*, Quantification showing the effect of CX3A on numbers of receptor clusters (α7-nAChRs: 9.7 ± 1.3 and 4.2 ± 0.7 clusters/20 μm for control and CX3A, respectively; GluR1s: 19.3 ± 2 and 19.9 ± 1.6 for control and CX3A, respectively; NR1s: 11.4 ± 1.3 and 9.7 ± 1.5 for control and CX3A, respectively; ***p = 0.0009 by two-tailed t test; n = 15–23 interneurons). *C*, Representative images of total PMCA2 expression in hippocampal neurons. Transfection (RFP, red) with a specific shPMCA2 construct reduces the expression of PMCA2 (PMCA2, green) compared with neighbor neurons and to shScramble-transfected neurons (shScr2). Scale bars: Top, left, 5 μm; bottom, left, 10 μm. (*D*) PMCA-dependent reduction in α7-nAChR cluster number is cell-autonomous as demonstrated by the lack of CX3A effects when PMCA2 is knocked down by RNAi (shPMCA2/CX3A) but not by scrambled control (shScr2/CX3A). Values for shScr2 were 8.7 ± 0.7 and 3.3 ± 0.6 for control and CX3A, respectively; and for shPMCA2: 7.6 ± 1.5 and 9 ± 2.8 for control and CX3A, respectively; ***p = 0.0008 by two-tailed t test; n = 10–12 interneurons.

A functional link between α7-nAChR and PMCA2
To test the effects of PMCA2 on α7-nAChR function, we loaded hippocampal neurons in culture with the calcium indicator Fluo-4 (Fig. 2*A*) and then focally activated α7-nAChRs by applying the specific agonist choline from a micropipette positioned 5 μm from the dendrite (Fig. 2*A*). A brief application of choline to an interneuron elicited calcium transients with magnitude and kinetics (Fig. 2*B*) comparable to those described previously using this technique (Fayuk and Yakel, 2007). These transients were not due to changes in cell volume (artifacts) caused by the choline puffs, as monitored by the distribution of soluble red fluorescent protein in the cell (Fig. 2*A,B*). A 1 h inhibition of PMCA2 activity by incubation with the peptide caloxin 3A (CX3A, 250 μM; Pande et

al., 2005) significantly slowed calcium clearance following α7-nAChR activation; this is reflected in the exponential fit of the decay phase of the calcium transient (Fig. 2*C*). Notably, PMCA2 inhibition by CX3A also produced a substantial decrease in the peak magnitude of the calcium response (Fig. 2*C*). An even greater decrement was observed with carboxyeosin (10 μM), another inhibitor of PMCA isoforms (Gatto et al., 1995; Fig. 2*C*). The results clearly suggest a functional association between PMCA2 and α7-nAChRs.

Dependence of surface α7-nAChRs on PMCA2 activity
The finding that PMCA2 inhibition reduced the magnitude of the rapid calcium transients generated by α7-nAChRs on interneurons raised the possibility that pump blockade might trigger re-

ceptor loss. To test this, we inhibited PMCA2 activity with CX3A and then labeled surface α7-nAChRs with Bgtx conjugated to Alexa Fluor 488 (Zago et al., 2006; Fig. 3A). Inhibition of PMCA2 significantly reduced the number of α7-nAChR clusters on the interneuron surface (Fig. 3B). No change was seen in the number of clusters comprising GluR1-containing AMPA receptors (GluR1s), another calcium-permeable receptor expressed by the same interneurons (Fig. 3A,B). Nor was any change seen in NR1-containing NMDA receptors (NR1s), a calcium-permeable receptor previously shown to be associated in part with PMCA2 in postsynaptic compartments (Garside et al., 2009). The results reveal a remarkable regulatory response of interneurons to control α7-nAChRs.

The physical association of PMCA2 with α7-nAChRs identified by proteomics and the proximity of the two proteins in the same dendrite shown by immunostaining suggested that the relevant PMCA2s mediating the loss of receptor clusters were on the same interneuron. The pump is known, however, to be distributed both presynaptically and postsynaptically (Jensen et al., 2007; Garside et al., 2009). We used RNAi to identify the relevant PMCA2 population. An shRNA construct for PMCA2 (shP-MCA2) dramatically reduced the amount of PMCA2 in the dendrites of interneurons expressing the construct (Fig. 3C) and prevented CX3A treatment from affecting the number of α7-nAChR clusters on the same dendrite (Fig. 3D). A scrambled shRNA control (shScr2) had no effect (Fig. 3D). The results confirm the specificity of the CX3A effect as being mediated by PMCA2 and demonstrate that the relevant PMCA2s are those on the same cell as the α7-nAChRs being regulated.

Mechanisms mediating the PMCA2 effect on α7-nAChRs
To identify signaling cascades mediating the PMCA2 effects on α7-nAChR cluster number, we tested whether increases in intracellular calcium were involved. After loading the neurons with the intracellular calcium chelator BAPTA-AM, we found that inhibition of PMCA2 no longer decreased the number of receptor clusters (Fig. 4A). Further, inhibition of calcium, calmodulin-dependent protein kinase II (CaMKII) with the specific blocker KN-93 also abolished the PMCA2-dependent loss of receptor clusters, whereas the inactive analog KN-92 had no effect (Fig. 4A). To test whether the regulatory effect depended on protein degradation, we blocked proteasome activity with MG132. This treatment prevented PMCA2-dependent loss of α7-nAChR clusters (Fig. 4A). The results suggest a homeostatic response to increases in calcium: PMCA2 inhibition allows intracellular calcium to increase, and the calcium elevation, acting through CaMKII, reduces the number of α7-nAChR clusters on the cell surface in a manner that depends on proteasome activity.

To identify the region of the α7-nAChR necessary for the PMCA2-dependent regulation, we used chimeras composed of nAChR fragments fused with the CD4 receptor (Xu et al., 2006; Fig. 4B). The second cytoplasmic loop of α3-containing nAChRs has previously been shown to be important for localizing such receptors on neurons (Williams et al., 1998). Accordingly, immunoprecipitation experiments were performed on extracts of transfected HEK293 cells expressing a chimera of the CD4 receptor fused with the second cytoplasmic loop of the α7-nAChR (CD4-α7). The α7-nAChR loop was sufficient for coimmunoprecipitation with PMCA2 (Fig. 4C). Substituting the equivalent region of the α4-nAChR subunit (CD4-α4) as a negative control did not permit coimmunoprecipitation with PMCA2.

To test whether the second intracellular loop was also sufficient for PMCA2-mediated loss of α7-nAChR surface clusters,
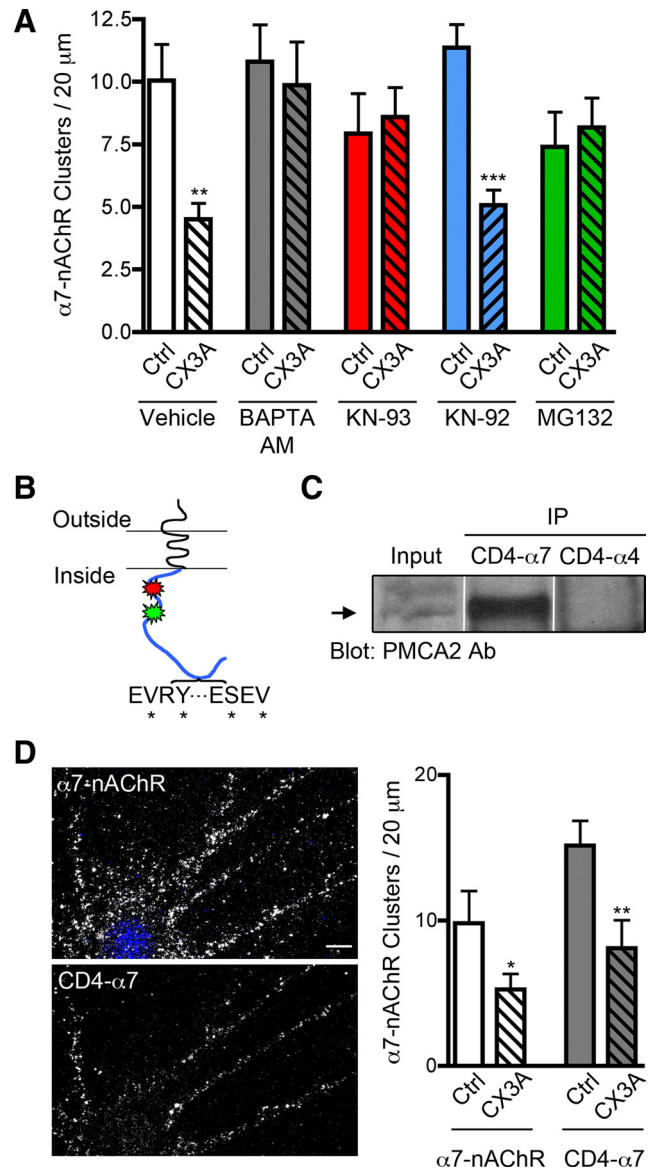

Figure 4. Molecular mechanisms mediating the PMCA2 effect on α7-nAChRs. *A*, The reduction in receptor clusters depends on changes in intracellular calcium concentration [blocked by BAPTA-AM; vehicle (DMSO): 10 ± 1.4 and 4.5 ± 0.6 for control (ctrl) and CX3A, respectively; BAPTA-AM: 10.8 ± 1.5 and 9.8 ± 1.7 for control and CX3A respectively; **p = 0.006 by two-tailed *t* test; *n* = 25 interneurons] and on CaMKII activity (blocked by KN93: 7.9 ± 1.6 and 8.6 ± 1.2 for control and CX3A, respectively; *n* = 23 interneurons; KN92 as negative control: 11.3 ± 0.9 and 5.06 ± 0.6 for control and CX3A, respectively; ***p = 0.0009 by two-tailed *t* test; *n* = 20 interneurons). The reduction also depends on proteasomal activity (blocked by MG132: 7.4 ± 1.4 and 8.2 ± 1.2 for control and CX3A, respectively; *n* = 27 interneurons). *B*, Schematic representation of a chimeric receptor containing the CD4 receptor extracellular and transmembrane domains (black line) and the second cytoplasmic loop sequence of α7-nAChR subunits (blue line). Consensus sequences for PKC and CKII are indicated by red and green symbols, respectively. PDZ motifs are indicated by their amino acid sequences. Asterisks indicate the position of mutated residues. *C*, Coimmunoprecipitation of PMCA2-Myc and CD4 chimeras transiently transfected into HEK293 cells. Proteins were immunopurified (IP) with Abs against the extracellular region of the CD4 sequence for both the CD-α7 and the CD4-α4 receptors. Arrow indicates the PMCA2-Myc band. Similar results were obtained from three independent experiments. *D*, Left, Representative images of surface endogenous α7-nAChRs or surface CD4-α7 on the same hippocampal interneuron (blue). Right, CX3A treatment reduces both the number of endogenous α7-nAChR clusters and transfected CD4-α7 clusters (α7-nAChRs: 9.8 ± 2.2 and 5.3 ± 1 for control and CX3A, respectively; *p = 0.039 by two-tailed *t* test; CD4α7-loop: 15.1 ± 1.7 and 8.1 ± 1.9 for control and CX3A, respectively; **p = 0.008 by two-tailed *t* test; *n* = 21–23 transfected interneurons).

we transfected hippocampal neurons in culture with the CD4-α7 loop (Fig. 4*D*) and inhibited PMCA2 activity. This resulted in loss of CD4-α7 loop clusters, as it did loss of endogenous α7-nAChR clusters (Fig. 4*D*). Candidate domains within the second intracellular loop of α7-nAChRs for mediating the PMCA2 effect include consensus motifs for protein kinase C (PKC), casein kinase II (CKII), and two type-1 PDZ domains (Fig. 4*B*). None of these appeared essential. Pharmacological blockade of either PKC with GF109203x or CKII with 4,5,6,7-tetrabromobenzotriazole (TBB) had no effect on either the control number of α7-nAChR clusters or the number remaining after PMCA2 inhibition [vehicle (DMSO): 10.2 ± 1.7 and 7 ± 1.2 for control and CX3A, respectively; GF109203x: 9.6 ± 1.4 and 4.5 ± 0.8 for control and CX3A, respectively; TBB: 9.1 ± 1.3 and 5.5 ± 1 for control and CX3A, respectively; $p < 0.05$ for DMSO and TBB by two-tailed t test; $p < 0.01$ for GF109203x by two-tailed t test; $n = 18–25$ interneurons; data not shown]. Though the PDZ domains might be expected to mediate protein interactions, mutating both the second and fourth residues to alanine in either or both PDZ domains had no effect on the ability of the chimeric construct to associate with PMCA2 as indicated by immunoprecipitation (data not shown). The results demonstrate that the second cytoplasmic loop of α7-nAChRs is required for interaction with and regulation by PMCA2, but that the PMCA2 association does not depend on previously identified binding motifs present in the loop.

Control of α7-nAChR lateral mobility by PSD-95

Close proximity of PMCA2s and α7-nAChRs within membrane microdomains is likely to be critical for the regulation observed. Scaffold proteins represent candidates for mediating this proximity. They previously have been shown to be associated with other nAChRs (Temburni et al., 2004; Rosenberg et al., 2008), and PSD-95 specifically has been reported to interact both with PMCA2 *in vivo* (DeMarco and Strehler, 2001; Garside et al., 2009) and with α7-nAChRs in cell culture (Farías et al., 2007). Pursuing this possibility, we identified an interaction between PSD-95 and α7-nAChR *in vivo* by coimmunoprecipitation from rat brain extracts (Fig. 5*A*). In addition, immunostaining showed that α7-nAChRs in part colocalize both with PSD-95 and with PMCA2 on hippocampal interneurons in culture (Fig. 5*B*).

To detect changes in receptor location within a membrane microdomain, we used SPT with QDs attached to α7-nAChRs. This technique provides the high localization accuracy needed for detecting changes in α7-nAChR location in a small area of plasma
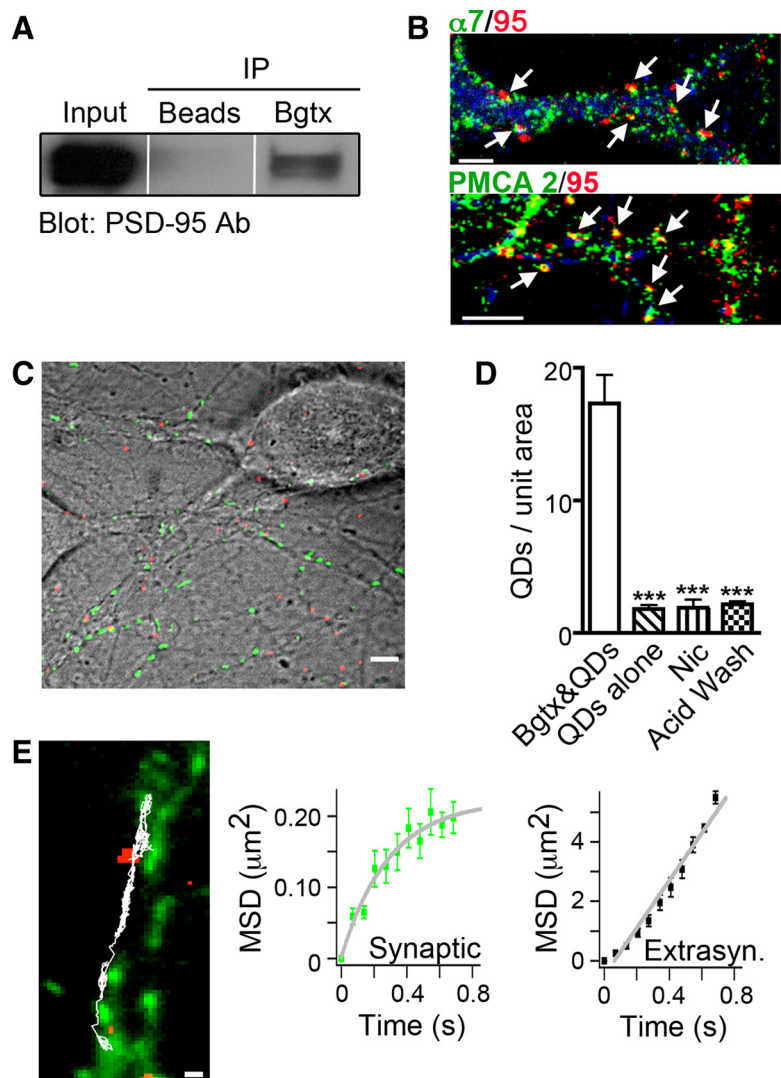

Figure 5. PSD-95 is associated with α7-nAChRs, and the receptors are constrained in synaptic space on aspiny neurons. **A**, Endogenous PSD-95 coaffinity purified with α7-nAChRs from rat brain extracts using the specific α7-nAChR agonist Bgtx attached to beads (Bgtx), and not by plain beads as a control (Beads). Equivalent results were obtained with six independent rat brain extracts. **B**, Top, Colocalization (arrows indicate examples) of surface α7-nAChRs (green) and PSD-95 (red) on hippocampal interneurons (GAD65, blue; 15–17 d *in vitro*). Bottom, Colocalization of PMCA2 (green) and PSD-95 (red) under the same conditions. Scale bars: 2 μm. **C**, Representative image of surface endogenous QD-α7-nAChR complexes (red) on hippocampal neurons (bright field image). Synapses were labeled using Mitotracker (green). Scale bar: 5 μm. **D**, Number of QD-α7-nAChR complexes on the surface of hippocampal neurons (Bgtx&QDs) compared with three control conditions: QDs without Bgtx (QDs alone), 100 μM nicotine added with the Bgtx to block binding (Nic), and Bgtx plus QDs but acid-stripped afterward to remove QDs from surface receptors (Acid Wash). Bgtx&QDs, 17.3 ± 2.2; QDs alone, 1.8 ± 0.3; Nic. comp., 1.9 ± 0.6; Acid Wash, 2.2 ± 0.2 (*** $p < 0.001$ by one-way ANOVA with *post hoc* Bonferroni test; $n = 15$ fields of view from 3 cultures). **E**, Left, Tracing showing the trajectory (white) of a postsynaptic α7-QD complex (red) during a 1 min recording. Synaptic locations were identified by transfected SAP-102-GFP (green). Scale bar: 1 μm. Right, MSD plots versus time for synaptic and extrasynaptic α7-QD movement.

membrane over time (Triller and Choquet, 2008). In this way, we examined the possibility that PSD-95 controls α7-nAChR position by constraining receptor lateral mobility in the plasma membrane, functionally linking them to PMCA2s in microdomains. The QDs were specifically attached to α7-nAChRs by using a streptavidin-conjugate that recognizes Bgtx biotin bound to the receptors (Fig. 5*C,D*). After transfecting aspiny neurons with SAP-102-GFP to label synapses, individual α7-nAChRs-QD complexes were tracked as they entered and exited synaptic space (Fig. 5*E*). MSD plots revealed that the receptor displayed random-walk diffusion in extrasynaptic space but became spatially constrained when in synapses (Fig. 5*E*). Quantification of
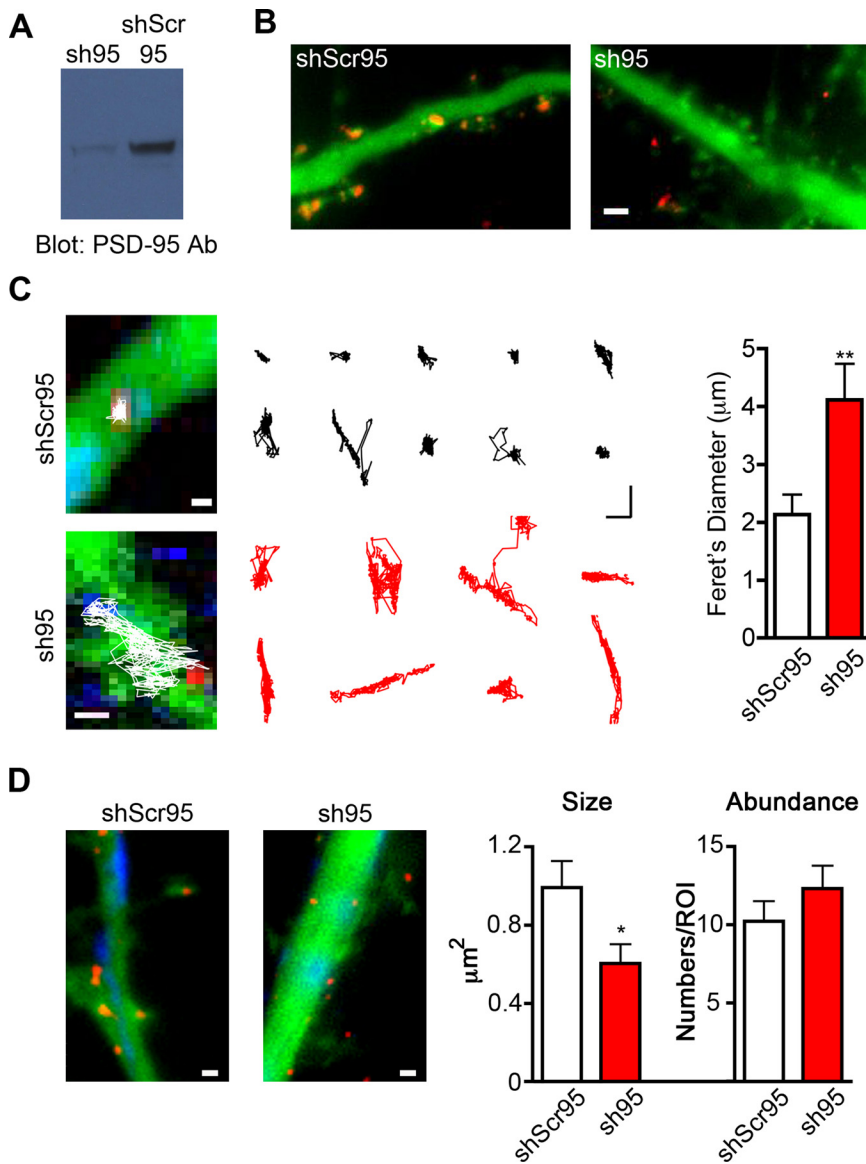
Figure 6. PSD-95 controls lateral mobility of α7-nAChR. **A**, Western blot of mouse PSD-95-GFP (dark band) transfected in HEK293 cells, together with sh95 or shScr95. **B**, Representative images of total endogenous PSD-95 (red) on hippocampal neurons transfected (green) with either shScr95 or sh95. Scale bar: 2 μm. **C**, Left, Tracings of the trajectories (white) of a postsynaptic α7-QD (red) on an aspiny neuron transfected with either shScr95 or sh95. Synapses are indicated by Mitotracker staining (blue). Scale bars: 1 μm. Right, Examples of α7-QD trajectories recorded on interneurons transfected either with shScr95 (black) or sh95 (red). Scale bars: 2 μm. Mean Feret's diameter values calculated for α7-QD complexes (2.1 $\pm$ 0.3 and 4.1 $\pm$ 0.6 μm for shScr95 and sh95, respectively; **p = 0.009 by two-tailed t test; n = 15 transfected interneurons from 3 cultures). **D**, PSD-95 knockdown reduces size of α7-nAChR clusters. Left, Representative images of surface α7-nAChRs (red) on interneurons (blue) transfected with either shScr95 or sh95 (green). Scale bars: 1 μm. Right, sh95 reduces surface α7-nAChR cluster size (0.99 $\pm$ 0.1 and 0.6 $\pm$ 0.1 μm^2 for shScr95 and sh95, respectively; *p = 0.03 for two-tailed t test; n = 12–16 transfected interneurons) but not α7-nAChR cluster number (10.2 $\pm$ 1.3 and 12.3 $\pm$ 1.4 for shScr95 and sh95, respectively; n = 12–16 transfected interneurons; ROI for quantification: 20 μm linear segment embedding the dendritic area).

diffusion coefficients demonstrated that receptor mobility was two times greater in extrasynaptic space than in synapses: 0.077 μm^2/s (IQR [interquartile range], 0.04–0.098 μm^2/s) and 0.165 μm^2/s (IQR, 0.095–0.2 μm^2/s) for synaptic and extrasynaptic space, respectively (n = 54, 60 trajectories; three cultures; p < 0.001, by Mann–Whitney test).

To test the role of PSD-95 in constraining receptor mobility, we again used RNAi. Knockdown of PSD-95, using a specific construct (sh95, Fig. 6A,B), enabled α7-nAChRs to diffuse more extensively in aspiny neurons as reflected by their tracks (Fig.

6C). Measuring the average distance between the two most distal points of the trajectory (Feret's diameter) indicated that α7-nAChRs on interneurons expressing sh95 moved twice as far on average as did α7-nAChRs on cells expressing the corresponding scrambled control shScr95 (Fig. 6C). Consistent with the changes observed in α7-nAChR mobility, we detected a reduced size of α7-nAChR clusters on the neuronal surface after PSD-95 knockdown and no change in the number of such clusters (Fig. 6D). PSD-95 knockdown by sh95 had no effect on the choline-induced calcium transients caused by α7-nAChRs, as expected (data not shown). The results identify PSD-95 as the first known protein to control the localization of α7-nAChRs on CNS neurons by means of limiting receptor mobility in the plasma membrane.

Role of PSD-95 in mediating PMCA2 control of α7-nAChRs

An early indication that PSD-95 might be involved in the PMCA2 regulation of α7-nAChR clusters came from the observation that treating cultures with CX3A caused a decrease in the size of the largest quartile of PSD-95 puncta ($-17 \pm 0.02\%$, n = 23 interneurons; $p \leq 0.01$) found on hippocampal interneurons. No change was seen in the other quartiles, and no change was seen in the total number of PSD-95 puncta (data not shown). This suggested that PMCA2 blockade may cause the loss of a specific population of PSD-95 molecules and their associated proteins. Conversely, downregulation of PSD-95 by expression of sh95 decreased the mean size of PMCA2 puncta without changing the number of such puncta ($-41 \pm 7\%$; n = 18 interneurons; $p \leq$ 0.01); this parallels the effect of sh95 on α7-nAChR clusters (see above).

To test directly whether PSD-95 is required for the loss of α7-nAChR clusters caused by PMCA2 inhibition, we examined hippocampal interneurons expressing sh95. Inhibition of PMCA2 with CX3A was unable to reduce the number of α7-nAChR clusters in this case (Fig. 7A,B). Importantly, PSD-95 knockdown did not alter the number of either α7-nAChR (Fig. 6B) or PMCA2 clusters (data not shown) under control conditions (i.e., in the absence of CX3A). These results demonstrate that PSD-95 is required for PMCA2-mediated loss of α7-nAChR clusters, apparently by constraining receptor mobility and functionally linking them to PMCA2 and regulatory machinery in the cell (Fig. 7C).

Discussion

The results presented here demonstrate a new mechanism for controlling local calcium dynamics in neurons. The ion channel

responsible for elevating intracellular calcium can be tightly coupled to a device capable of removing the calcium that enters and limits its spread. Further, the coupling can be used to target the ion channel for removal from the site if local calcium levels exceed a critical threshold. For α7-nAChRs on interneurons, the coupling is provided by PSD-95, which functionally links the receptors to PMCA2. If the calcium pump is unable to limit local calcium elevations, as in the case of pump inhibition, the cell quickly eliminates the α7-nAChR clusters. The regulation appears dedicated in that it does not extend either to GluR1-containing or NR1-containing receptors on the same neurons; both types are calcium-permeable and reported to interact with PSD-95 and calcium pumps (Goldberg et al., 2003; Garside et al., 2009).

Previous studies showed that PMCA proteins participate in multiprotein calcium signaling complexes (Strehler et al., 2007). Several PMCA2 isoforms have been shown to interact with synapse-associated PDZ-contained proteins, including members of the PSD-95 family (DeMarco and Strehler, 2001). In rat cerebellum, postsynaptic PMCA2 interacts with NR1-containing and NR2-containing NMDA receptors (Garside et al., 2009). These findings suggest that PMCA2 localization may be used to promote calcium homeostasis in membrane microdomains containing calcium-permeable ligand-gated ion channels.

Functional proteomics has emerged as a powerful strategy for identifying proteins comprising molecular networks to regulate neuronal receptors (Schulte et al., 2011). Though large-scale screening of interactive proteins has recently been extended to nAChRs, functional interactions have yet to be identified this way (Kabbani et al., 2007; Paulo et al., 2009). Using an unbiased proteomic approach, we show here that α7-nAChRs are functionally tethered to PMCA2 and, together with PSD-95, the components form a functional unit that achieves two kinds of regulation. The first is an immediate constraint of calcium spread following α7-nAChR activation, reminiscent of that achieved by the interplay between calcium-permeable AMPA receptors and a Na^+/Ca^{2+} exchanger in neocortical fast-spiking interneurons to localize calcium in microdomains (Goldberg et al., 2003). The second, and more radical, is rapid loss of α7-nAChR clusters in response to PMCA2 blockade, suggesting a homeostatic mechanism for controlling calcium levels similar to that reported for AMPA receptor loss following Na^+/K^+-ATPase pump blockade on pyramidal neurons (Zhang et al., 2009).

Imaging techniques have been used to assess trafficking of nAChRs to the plasma membrane from interior locations (Nashmi et al., 2003; Richards et al., 2011). Recent studies using
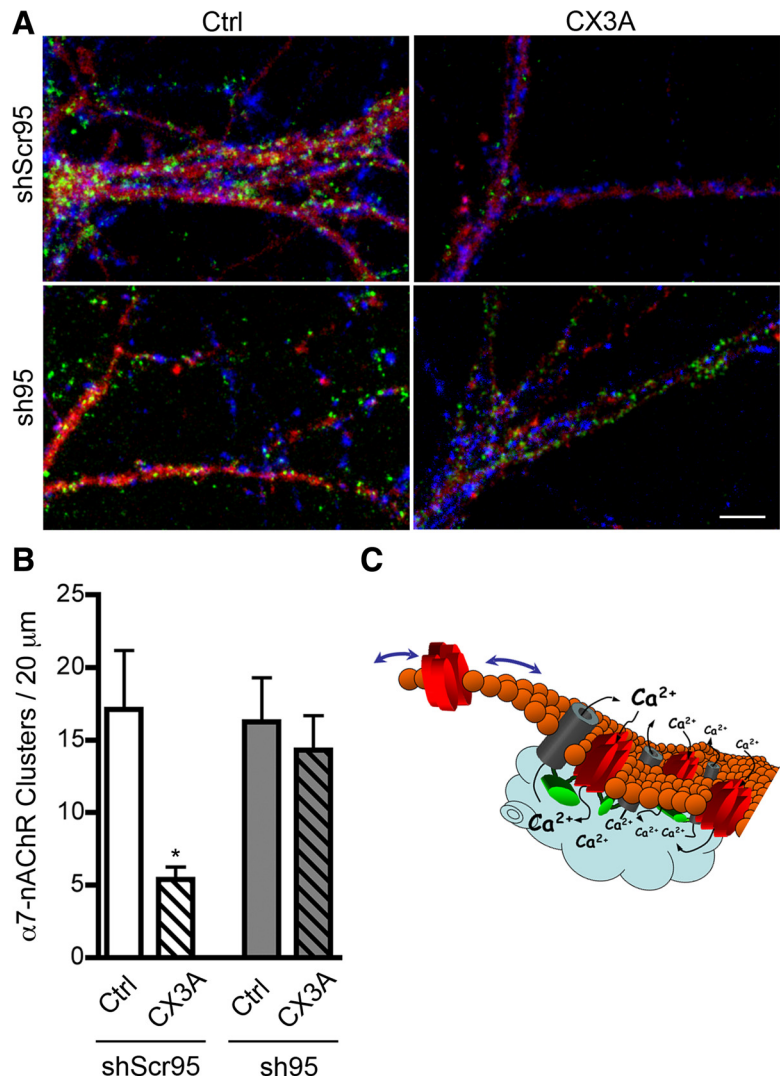

Figure 7. PSD95 knock-down abolishes PMCA2-dependent loss of α7-nAChR clusters. **A**, Images of interneurons immunostained for GAD-65 (blue) and costained for surface α7-nAChRs (green) after transfection either with shScr95 or sh95 (red) and treated with vehicle (Ctrl) or CX3A. Scale bar: 5 μm. **B**, PMCA2 inhibition by CX3A reduces the number of α7-nAChRs clusters on interneurons transfected with shScr95 but not with sh95 (shScr95: 17.1 ± 4.1 and 5.4 ± 0.9 clusters/20 μm for control (Ctrl) and CX3A, respectively; *p = 0.01 by two-tailed t test; sh95: 16.2 ± 3 and 14.3 ± 2.4 for control and CX3A, respectively; n = 18 –21 transfected interneurons). **C**, Model of an aspiny interneuron dendrite showing the α7-nAChR/PMCA2/PSD-95 complex (red/gray/green, respectively). Black solid arrows indicate the movement of calcium. Double-headed blue arrows represent the mobility of α7-nAChRs in the surface membrane. Blue cloud represents a calcium microdomain created by the orchestrated activity of the α7-nAChR/PMCA2/PSD-95 complex.

SPT have shown that α7-nACRs are mobile on the neuron surface but display constraint in synaptic/perisynaptic domains (Bürli et al., 2010; Fernandes et al., 2010). The receptors interact with several scaffold proteins including PSD-93, PSD-95, PICK1 (protein interacting with C kinase-1), and APC (adenomatous polyposis coli) depending on location (Conroy et al., 2003; Baer et al., 2007; Farías et al., 2007). Axotomy-induced synaptic degeneration disperses postsynaptic PSD-93 before mobilizing α7-nACRs, consistent with a functional interaction (McCann et al., 2008). Recently, it has been shown that specific disruption of PDZ-containing scaffolds increases α7-nACR mobility on avian neurons (Fernandes et al., 2010). The SPT studies reported here identify PSD-95 as the first protein that constrains α7-nACR mobility on the neuron surface and functionally links the receptors to PMCA2. This link mediates regulation of α7-nACRs by PMCA2.

To achieve the regulation seen, the PMCA2/α7-nAChR complex must be positioned in microdomains where appropriate cellular machinery can eliminate α7-nAChR clusters in a calcium-dependent manner, as occurs when PMCA2 is inhibited. This requires participation of additional components, possibly also tethered to the complex. CaMKII may be one such a component. Activation of CaMKII can enhance receptor trafficking in the membrane and promote recycling (Derkach et al., 1999; Malinow and Malenka, 2002). Moreover, CaMKII can phosphorylate PSD-95, controlling the association between PSD-95 and NMDA2A receptors (Gardoni et al., 2006; Tsui and Malenka, 2006). We show here that CaMKII is required for loss of α7-nAChR clusters following PMCA2 inactivation, and may determine the local precision of the response. Only those domains experiencing elevated calcium will activate CaMKII, and only those activated complexes also positioned near appropriate cellular machinery will remove α7-nAChR clusters. Notably, calcium influx through α7-nAChRs themselves is not required because CX3A treatment induces cluster loss even when the receptors are prelabeled with Alexa488-Bgtx and methyllycaconitine is added, blocking their function (data not shown). Rather, it is PMCA2 inactivation that induces loss of associated α7-nAChR clusters in a calcium-dependent and CaMKII-dependent manner.

Loss of α7-nAChR clusters following PMCA2 inhibition depended on proteasomal degradation. Proteasomal activity has previously been shown to regulate the number and stability of nicotinic receptors (Rezvani et al., 2007; Govind et al., 2012). The loss of α7-nAChR clusters here may reflect either their internalization or dispersal on the cell surface. Current methods of immunodetection do not allow us to distinguish between extensive dispersal of clusters on the surface versus receptor internalization. We can detect small changes in cluster size, as in the case of sh95-treated neurons, and these produce no change in the choline-induced calcium response (data not shown). The large decrements in response caused by CX3A treatment, together with the substantial reduction in number of clusters, therefore suggests either complete (radical) dispersal or, more likely, receptor internalization. In either case, proteasomal dependency may also reflect a requirement for proteasomal degradation and turnover of regulatory components affecting α7-nAChR location on the surface. The proteasome has previously been shown to be essential for removal of calcium-permeable ion channels when a specific ion pump was inhibited (Zhang et al., 2009). PMCA2 is also known to be degraded by the proteasome when ATP production is compromised (Mbaya et al., 2010).

The physical association of PMCA2 with α7-nAChRs may identify the complex as a target for the proteasome when the pump is inhibited by CX3A. This physical association depends on the second intracellular loop of the α7-nAChR subunit but does not require any of the sequences identified as potential binding/regulatory motifs. The loop likely connects the α7-nAChR to the PSD-95 scaffold, as has been suggested for the receptor link to PICK1 (Baer et al., 2007). The ability to coimmunoprecipitate PMCA2 with α7-nAChRs when both are expressed in transfected HEK cells may reflect the presence of an endogenous scaffold protein that can link the two. HEK cells express SAP-97, for example, a member of the PSD-95 family (Sabio et al., 2005).

Importantly, not all PMCA2/PSD-95 complexes with calcium-permeable receptors display the regulatory response to calcium elevations seen here for α7-nAChRs. As noted above, neither GluR1-containing AMPA receptor clusters nor NMDA receptor clusters containing NR1 receptors were dispersed by

PMCA2 blockade though both classes of receptors have been shown previously to interact with PSD-95, and at least NMRA receptors have been shown to be associated with PMCA2 (Garside et al., 2009). Notably, CX3A blockade of PMCA2 decreased the size of the largest PSD-95 puncta without changing the total number of PSD-95 puncta. Individual microdomains of such puncta presumably reflect unique regulatory units, depending on the components and receptors attached.

It may seem paradoxical that knockdown of PMCA2 by RNAi did not produce loss of α7-nAChR clusters, in contrast to the effects PMCA2 blockade by CX3A. PMCA2 knockdown, however, is usually less than complete and requires multiple days; this could induce compensatory changes, perhaps increasing other PMCAs known to be in hippocampal neurons (Marcos et al., 2009). PMCA knockdown, for example, was shown recently to increase calmodulin levels (Boczek et al., 2012), relevant here because CaMKII mediates the α7-nAChR loss observed. An interesting alternative is that the physical presence of PMCA2, as noted above, may be needed as part of the signaling complex triggering loss of α7-nAChR clusters when intracellular calcium levels increase.

Previous work has shown that α7-nAChRs can also occupy presynaptic positions at a variety of locations (McGehee et al., 1995; Gray et al., 1996; Alkondon and Albuquerque, 2001; Sharma and Vijayaraghavan, 2003), as does PMCA2 (Garside et al., 2009). Here we focused on postsynaptic α7-nAChRs and their interactions with PMCA2. The role of presynaptic α7-nAChRs, however, and their dependence on calcium to influence transmitter release raises obvious questions about possible α7-nAChRs/PMCA2 interactions similar to those identified here on the postsynaptic side. This will be important to address when imaging techniques are available to visualize presynaptic α7-nAChRs.

The calcium regulatory mechanisms identified here may be particularly important in cellular domains where physical compartmentalization is difficult, as in the case of dendritic shafts on aspiny interneurons. Though interneurons were originally thought only to regulate the flow of excitability generated by pyramidal neurons, it is now clear that the cells display multiple forms of plasticity, some of which are pathway-specific (Kullmann and Lamsa, 2007). The mechanisms required for constraining calcium fluctuations to microdomains remain largely unexplored (Kullmann and Lamsa, 2007; Michaelsen and Lohmann, 2010). Regulation of calcium dynamics by the orchestrated activity of specific protein complexes, like the one shown here, offers an additional possibility. Future interactomics studies on other neuronal receptors will help determine whether the principles identified here are fundamental to the regulation of calcium dynamics where physical compartmentalization is not available.

References

Albuquerque EX, Pereira EF, Alkondon M, Rogers SW (2009) Mammalian nicotinic acetylcholine receptors: from structure to function. Physiol Rev 89:73–120.

Alkondon M, Albuquerque EX (2001) Nicotinic acetylcholine receptors α7 and α4β2 subtypes differentially control GABAergic input to CA1 neurons in rat hippocampus. J Neurophysiol 86:3043–3055.

Aravanis AM, Pyle JL, Tsien RW (2003) Single synaptic vesicles fusing transiently and successively without loss of identity. Nature 423:643–647.

Baer K, Bürli T, Huh KH, Wiesner A, Erb-Vögtli S, Göckeritz-Dujmovic D, Moransard M, Nishimune A, Rees MI, Henley JM, Fritschy JM, Fuhrer C (2007) PICK1 interacts with alpha7 neuronal nicotinic acetylcholine receptors and controls their clustering. Mol Cell Neurosci 35:339–355.

Bertrand D, Galzi JL, Devillers-Thiéry A, Bertrand S, Changeux JP (1993) Mutations at two distinct sites within the channel domain M2 alter cal-

cium permeability of neuronal alpha 7 nicotinic receptor. Proc Natl Acad Sci U S A 90:6971–6975.

Boczek T, Kozaczuk A, Ferenc B, Kosiorek M, Pikula S, Zylinska L (2012) Gene expression pattern in PC12 cells with reduced PMCA2 or PMCA3 isoform: selective up-regulation of calmodulin and neuromodulin. Mol Cell Biochem 360:89–102.

Bürli T, Baer K, Ewers H, Sidler C, Fuhrer C, Fritschy JM (2010) Single particle tracking of alpha7 nicotinic AChR in hippocampal neurons reveals regulated confinement at glutamatergic and GABAergic perisynaptic sites. PLoS One 5:e11507.

Charrier C, Ehrensperger MV, Dahan M, Lévi S, Triller A (2006) Cytoskeleton regulation of glycine receptor number at synapses and diffusion in the plasma membrane. J Neurosci 26:8502–8511.

Conroy WG, Liu Z, Nai Q, Coggan JS, Berg DK (2003) PDZ-containing proteins provide a functional postsynaptic scaffold for nicotinic receptors in neurons. Neuron 38:759–771.

Dajas-Bailador F, Wonnacott S (2004) Nicotinic acetylcholine receptors and the regulation of neuronal signalling. TIPS 25:317–324.

DeMarco SJ, Strehler EE (2001) Plasma membrane Ca^{2+}-atpase isoforms 2b and 4b interact promiscuously and selectively with members of the membrane-associated guanylate kinase family of PDZ (PSD95/Dlg/ZO-1) domain-containing proteins. J Biol Chem 276:21594–21600.

Derkach V, Barria A, Soderling TR (1999) Ca^{2+}/calmodulin-kinase II enhances channel conductance of alpha-amino-3-hydroxy-5-methyl-4-isoxazolepropionate type glutamate receptors. Proc Natl Acad Sci U S A 96:3269–3274.

Descarries L, Gisiger V, Steriade M (1997) Diffuse transmission by acetylcholine in the CNS. Prog Neurobiol 53:603–625.

Dickinson JA, Hanrott KE, Mok MH, Kew JN, Wonnacott S (2007) Differential coupling of α7 and nonα7 nicotinic acetylcholine receptors to calcium-induced calcium release and voltage-operated calcium channels in PC12 cells. J Neurochem 100:1089–1096.

Dingledine R, Borges K, Bowie D, Traynelis SF (1999) The glutamate receptor ion channels. Pharmacol Rev 51:7–61.

Ehlers MD, Heine M, Groc L, Lee MC, Choquet D (2007) Diffusional trapping of GluR1 AMPA receptors by input-specific synaptic activity. Neuron 54:447–460.

Farías GG, Vallés AS, Colombres M, Godoy JA, Toledo EM, Lukas RJ, Barrantes FJ, Inestrosa NC (2007) Wnt-7a induces presynaptic colocalization of alpha 7-nicotinic acetylcholine receptors and adenomatous polyposis coli in hippocampal neurons. J Neurosci 27:5313–5325.

Fayuk D, Yakel JL (2007) Dendritic Ca^{2+} signalling due to activation of alpha 7-containing nicotinic acetylcholine receptors in rat hippocampal neurons. J Physiol 582:597–611.

Fernandes CC, Berg DK, Gómez-Varela D (2010) Lateral mobility of nicotinic acetylcholine receptors on neurons is determined by receptor composition, local domain, and cell type. J Neurosci 30:8841–8851.

Gardoni F, Polli F, Cattabeni F, Di Luca M (2006) Calcium-calmodulin-dependent protein kinase II phosphorylation modulates PSD-95 binding to NMDA receptors. Eur J Neurosci 24:2694–2704.

Garside ML, Turner PR, Austen B, Strehler EE, Beesley PW, Empson RM (2009) Molecular interactions of the plasma membrane calcium ATPase 2 at pre- and post-synaptic sites in rat cerebellum. Neuroscience 162:383–395.

Gatto C, Hale CC, Xu W, Milanick MA (1995) Eosin, a potent inhibitor of the plasma membrane Ca pump, does not inhibit the cardiac Na-Ca exchanger. Biochemistry 34:965–972.

Goetze B, Grunewald B, Baldassa S, Kiebler M (2004) Chemically controlled formation of a DNA/calcium phosphate coprecipitate: application for transfection of mature hippocampal neurons. J Neurobiol 60:517–525.

Goldberg JH, Tamas G, Aronov D, Yuste R (2003) Calcium microdomains in aspiny dendrites. Neuron 40:807–821.

Gómez-Varela D, Kohl T, Schmidt M, Rubio ME, Kawabe H, Nehring RB, Schäfer S, Stühmer W, Pardo LA (2010) Characterization of Eag1 channel lateral mobility in rat hippocampal cultures by single-particle-tracking with quantum dots. PLoS One 5:e8858.

Govind AP, Walsh H, Green WN (2012) Nicotine-induced upregulation of native neuronal nicotinic receptors is caused by multiple mechanisms. J Neurosci 32:2227–2238.

Gray R, Rajan AS, Radcliffe KA, Yakehiro M, Dani JA (1996) Hippocampal synaptic transmission enhanced by low concentrations of nicotine. Nature 383:713–716.

Jensen TP, Filoteo AG, Knopfel T, Empson RM (2007) Presynaptic plasma membrane Ca2+ ATPase isoform 2a regulates excitatory synaptic transmission in rat hippocampal CA3. J Physiol 579:85–99.

Jones S, Sudweeks S, Yakel JL (1999) Nictinic receptors in the brain: correlating physiology with function. Trends Neurosci 22:555–561.

Kabbani N, Woll MP, Levenson R, Lindstrom JM, Changeux JP (2007) Intracellular complexes of the beta2 subunit of the nicotinic acetylcholine receptor in brain identified by proteomics. Proc Natl Acad Sci U S A 104:20570–20575.

Kaeser PS, Deng L, Wang Y, Dulubova I, Liu X, Rizo J, Südhof TC (2011) RIM proteins tether Ca2+ channels to presynaptic active zones via a direct PDZ-domain interaction. Cell 144:282–295.

Kawai H, Zago W, Berg DK (2002) Nicotinic alpha 7 receptor clusters on hippocampal GABAergic neurons: regulation by synaptic activity and neurotrophins. J Neurosci 22:7903–7912.

Keller A, Nesvizhskii AI, Kolker E, Aebersold R (2002) Empirical statistical model to estimate the accuracy of peptide identifications made by MS/MS and database search. Anal Chem 74:5383–5392.

Khiroug L, Giniatullin R, Klein RC, Fayuk D, Yakel JL (2003) Functional mapping and Ca^{2+} regulation of nicotinic acetylcholine receptor channels in rat hippocampal CA1 neurons. J Neurosci 23:9024–9031.

Kozel PJ, Friedman RA, Erway LC, Yamoah EN, Liu LH, Riddle T, Duffy JJ, Doetschman T, Miller ML, Cardell EL, Shull GE (1998) Balance and hearing deficits in mice with a null mutation in the gene encoding plasma membrane Ca2+-ATPase isoform 2. J Biol Chem 273:18693–18696.

Kullmann DM, Lamsa KP (2007) Long-term synaptic plasticity in hippocampal interneurons. Nat Rev Neurosci 8:687–699.

Malinow R, Malenka RC (2002) AMPA receptor trafficking and synaptic plasticity. Annu Rev Neurosci 25:103–126.

Marcos D, Sepulveda MR, Berrocal M, Mata AM (2009) Ontogeny of ATP hydrolysis and isoform expression of the plasma membrane Ca^{2+}-ATPase in mouse brain. BMC Neurosci 10:112.

Mbaya E, Oulès B, Caspersen C, Tacine R, Massinet H, Pennuto M, Chrétien D, Munnich A, Rötig A, Rizzuto R, Rutter GA, Paterlini-Bréchot P, Chami M (2010) Calcium signalling-dependent mitochondrial dysfunction and bioenergetics regulation in respiratory chain Complex II deficiency. Cell Death Differ 17:1855–1866.

McCann CM, Tapia JC, Kim H, Coggan JS, Lichtman JW (2008) Rapid and midifiable neurotransmitter receptor dynamics at a neuronal synapse in vivo. Nat Neurosci 11:807–815.

McGehee DS, Heath MJ, Gelber S, Devay P, Role LW (1995) Nicotine enhancement of fast excitatory synaptic transmission in CNS by presynaptic receptors. Science 269:1692–1696.

Michaelsen K, Lohmann C (2010) Calcium dynamics at developing synapses: mechanisms and functions. Eur J Neurosci 32:218–223.

Miwa JM, Freedman R, Lester HA (2011) Neural systems governed by nicotinic acetylcholine receptors: emerging hypotheses. Neuron 70:20–33.

Nashmi R, Dickinson ME, McKinney S, Jareb M, Labarca C, Fraser SE, Lester HA (2003) Assembly of α4β2 nicotinic acetylcholine receptors assessed with functional fluorescently labeled subunits: effects of localization, trafficking, and nicotine-induced upregulation in clonal mammalian cells and in cultured midbrain neurons. J Neurosci 23:11554–11567.

Neff RA 3rd, Conroy WG, Schoellerman JD, Berg DK (2009) Synchronous and asynchronous transmitter release at nicotinic synapses are differentially regulated by postsynaptic PSD-95 proteins. J Neurosci 29:15770–15779.

Nesvizhskii AI, Keller A, Kolker E, Aebersold R (2003) A statistical model for identifying proteins by tandem mass spectrometry. Anal Chem 75:4646–4658.

Pande J, Mallhi KK, Grover AK (2005) Role of third extracellular domain of plasma membrane Ca2+-Mg2+-ATPase based on the novel inhibitor caloxin 3A1. Cell Calcium 37:245–250.

Paulo JA, Brucker WJ, Hawrot E (2009) Proteomic analysis of an alpha7 nicotinic acetylcholine receptor interactome. J Proteome Res 8:1849–1858.

Rezvani K, Teng Y, Shim D, De Biasi M (2007) Nicotine regulates multiple synaptic proteins by inhibiting proteasomal activity. J Neurosci 27:10508–10519.

Richards CI, Srinivasan R, Xiao C, Mackey ED, Miwa JM, Lester HA (2011) Trafficking of α4* nicotinic receptors revealed by superecliptic phluorin. Effects of a β4 amyotrophic lateral sclerosis-associated mutation and chronic exposure to nicotine. J Biol Chem 286:31241–31249.

Rosenberg MM, Yang F, Giovanni M, Mohn JL, Temburni MK, Jacob MH (2008) Adenomatous polyposis coli plays a key role, in vivo, in coordinating assembly of the neuronal nicotinic postsynaptic complex. Mol Cell Neurosci 38:138–152.

Rózsa B, Katona G, Kaszás A, Szipöcs R, Vizi ES (2008) Dendritic nicotinic receptors modulate backpropagating action potentials and long-term plasticity of interneurons. Eur J Neurosci 27:364–377.

Sabio G, Arthur JS, Kuma Y, Peggie M, Carr J, Murray-Tait V, Centeno F, Goedert M, Morrice NA, Cuenda A (2005) p38gamma regulates the localisation of SAP97 in the cytoskeleton by modulating its interaction with GKAP. EMBO J 24:1134–1145.

Sage D, Neumann FR, Hediger F, Gasser SM, Unser M (2005) Automatic tracking of individual fluorescence particles: application to the study of chromosome dynamics. IEEE Trans Image Process 14:1372–1383.

Schiller J, Schiller Y, Clapham DE (1998) NMDA receptors amplify calcium influx into dendritic spines during associative pre- and postsynaptic activation. Nat Neurosci 1:114–118.

Schulte U, Müller CS, Fakler B (2011) Ion channels and their molecular environments–glimpses and insights from functional proteomics. Semin Cell Dev Biol 22:132–144.

Séguéla P, Wadiche J, Dineley-Miller K, Dani JA, Patrick JW (1993) Molecular cloning, functional properties, and distribution of rat brain α_7: a nicotinic cation channel highly permeable to calcium. J Neurosci 13:596–604.

Sharma G, Vijayaraghavan S (2003) Modulation of presynaptic store calcium induces release of glutamate and postsynaptic firing. Neuron 38:929–939.

Strehler EE, Zacharias DA (2001) Role of alternative splicing in generating isoform diversity among plasma membrane calcium pumps. Physiol Rev 81:21–50.

Strehler EE, Filoteo AG, Penniston JT, Caride AJ (2007) Plasma-membrane Ca(2+) pumps: structural diversity as the basis for functional versatility. Biochem Soc Trans 35:919–922.

Temburni MK, Rosenberg MM, Pathak N, McConnell R, Jacob MH (2004) Neuronal nicotinic synapse assembly requires the adenomatous polyposis coli tumor suppressor protein. J Neurosci 24:6776–6784.

Triller A, Choquet D (2008) New concepts in synaptic biology derived from single-molecule imaging. Neuron 59:359–374.

Tsui J, Malenka RC (2006) Substrate localization creates specificity in calcium/calmodulin-dependent protein kinase II signaling at synapses. J Biol Chem 281:13794–13804.

Williams BM, Temburni MK, Levey MS, Bertrand S, Bertrand D, Jacob MH (1998) The long internal loop of the $\alpha3$ subunit targets nAChRs to subdomains within individual synapses on neurons in vivo. Nat Neurosci 1:557–562.

Xu J, Zhu Y, Heinemann SF (2006) Identification of sequence motifs that target neuronal nicotinic receptors to dendrites and axons. J Neurosci 26:9780–9793.

Yuste R (2011) Dendritic spines and distributed circuits. Neuron 71:772–781.

Yuste R, Majewska A, Cash SS, Denk W (1999) Mechanisms of calcium influx into hippocampal spines: heterogeneity among spines, coincidence detection by NMDA receptors, and optical quantal analysis. J Neurosci 19:1976–1987.

Zago WM, Massey KA, Berg DK (2006) Nicotinic activity stabilizes convergence of nicotinic and GABAergic synapses on filopodia of hippocampal interneurons. Mol Cell Neurosci 31:549–559.

Zhang D, Hou Q, Wang M, Lin A, Jarzylo L, Navis A, Raissi A, Liu F, Man HY (2009) Na,K-ATPase activity regulates AMPA receptor turnover through proteasome-mediated proteolysis. J Neurosci 29:4498–4511.